A Blind Restoration Method for Remote Sensing Images

Huanfeng Shen, Lijun Du, Liangpei Zhang, and Wei Gong

***Abstract*—This letter proposes a blind image restoration method for the deblurring of remote sensing images. A simple but robust identification method of point spread function (PSF) support is proposed, and a joint estimation method is presented to simultaneously solve the PSF coefficients and restoration image. To narrow the solution space for the best possible definition, the Huber–Markov (Huber–Markov random field) prior model is employed to regularize the two series of unknowns. Experiments were performed to demonstrate the effectiveness of the proposed approach.**

***Index Terms*—Blind restoration, joint estimation, support identification.**

I. Introduction

In MANY cases, the blurring of remote sensing images is unavoidable. It can be the result of atmospheric turbulence, scattering, spacecraft motion, aberrations, the lens being out of focus, and other properties of the sensor and atmosphere. It is, therefore, necessary for remote sensing users to deblur the degraded images using image restoration methods. Generally, the fuzziness of the imaging system can be described as

$$\boldsymbol{g} = \boldsymbol{H}\boldsymbol{f} + \boldsymbol{n} \tag{1}$$

where $\boldsymbol{f}$ and $\boldsymbol{g}$ represent the original image and degraded image, respectively, lexicographically ordered by stacking the rows of each image into a vector. $\boldsymbol{H}$ is a block–circulant-circulant-block matrix constructed from the point spread function (PSF), and $\boldsymbol{n}$ represents the noise vector.

A nonblind image restoration technique estimates the desired image $\boldsymbol{f}$, given the degraded image $\boldsymbol{g}$ and the PSF $\boldsymbol{h}$. The Richardson–Lucy method [1], [2] was widely adopted in the early applications of image restoration. The Wiener filter is another classical method, which is still frequently used to restore remote sensing images, because of its high efficiency [3]. Furthermore, the regularization method [4], maximum *a posteriori* (MAP) approach [5], and projections onto convex sets method [6] have also been popular restoration frameworks. Recently, some new signal processing techniques, such as sparse representation [7] and nonlocal means [8], have also been applied to the image restoration problem.

Blind restoration techniques estimate both the PSF $\boldsymbol{h}$ and the desired image $\boldsymbol{f}$, given the observed image $\boldsymbol{g}$. They can be classified into two categories, according to the stage at which the blur is identified: *a priori* or jointly with the image. In the former class of method, the PSF is identified prior to the restoration. An early research project [9] used the phase information of the image to estimate the PSF in the frequency domain. Remote sensing researchers often characterize the PSF using special features (point source, edges, etc.) of the blurred image, and the commonly used methods include the knife-edge method [10], the tarp-based target method [10], and the pulse method [11]. A more recent study used a marginal likelihood optimization (MLO) method to estimate the PSF prior to the image and validated that it is more robust than some joint methods [12]. The majority of existing methods fall into the latter class of joint method, where the image and blur are identified simultaneously. Ayers and Dainty [13] proposed an iterative blind deconvolution (IBD) algorithm to estimate the image and blur in the frequency domain. Fish *et al.* extended the classical Richardson–Lucy method to a blind approach [14]. The maximum likelihood deconvolution (MLD) restoration method is presented in [15]. You and Kaveh proposed a regularization method [4], and Chen *et al.* [16] proposed a MAP method in the wavelet domain. It is noted that most blind restoration methods to date have set the PSF support at an assumed size.

This letter proposes a new blind image restoration method for the deblurring of remote sensing images. First, we propose a simple but robust PSF support estimation method. Second, a joint estimation method based on a MAP framework is proposed to simultaneously solve the PSF coefficients and restoration image. For the first time, the Huber–Markov prior model is used to regularize both the image and the blur parameters.

II. PSF Support Identification

The shape of the PSF is often considered to be rectangular, and the horizontal and vertical measurements, respectively, should be estimated. Chen and Yap [17] developed a technique that minimizes the autocorrelation of a filtered image to identify the PSF support. The filtered image is obtained by convoluting the degraded image with a filter constructed from autoregressive (AR) model coefficients. This technique involves the intractable problem of obtaining the solution for AR coefficients and is not reliable for images with nonhomogeneous textures.

Inspired by [17], we have designed a simplified support estimation method. The main difference between this method and that of [17] is the design of the two fixed filters to replace

Manuscript received April 16, 2011; revised July 22, 2011, October 25, 2011, and February 20, 2012; accepted February 26, 2012. This work was supported in part by Major State Basic Research Development Program (973) under Grant 2011CB707103, by the National Natural Science Foundation of China under Grants 40971220 and 41071269, and by the Hubei Natural Science Foundation under Grant 2011CDA096.

H. Shen and L. Du are with the School of Resource and Environmental Science, Wuhan University, Wuhan 430079, China (e-mail: shenhf@whu.edu.cn; duzi276@163.com).

L. Zhang and W. Gong are with The State Key Laboratory of Information Engineering in Surveying, Mapping, and Remote Sensing, Wuhan University, Wuhan 430079, China (e-mail: zlp62@lmars.whu.edu.cn; weigong@lmars.whu.edu.cn).

Color versions of one or more of the figures in this paper are available online at http://ieeexplore.ieee.org.

Digital Object Identifier 10.1109/LGRS.2012.2190038

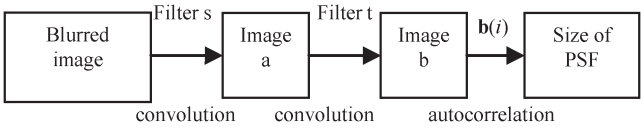

Fig. 1. Schema of the PSF support identification.

the filter produced by the AR model. Fig. 1 is the schema of the proposed estimation process.

In Fig. 1, Image $\boldsymbol{b}(i)$ denotes the shifted version of the image by shifting i pixels in horizontal or vertical directions. The filter s and the filter t are assigned to

$$\begin{bmatrix} -0.5 & -1 & -0.5 \\ -1 & 6 & -1 \\ -0.5 & -1 & -0.5 \end{bmatrix} \qquad \begin{bmatrix} 0 & 1 & 0 \\ 1 & -5 & 1 \\ 0 & 1 & 0 \end{bmatrix}$$

respectively. The former has a characteristic of high-pass filtering, removing much low-frequency information so that the main object of the operations is focused on the edge areas, while the latter highlights the characteristics of the image edge areas, to cause more obvious peaks in the autocorrelation curve. The determination of the PSF support is given as follows:

$$v\_size = \arg_m \min\left(J(m,0)\right) \tag{2}$$
$$h\_size = \arg_n \min\left(J(0,n)\right) \tag{3}$$

where v_size and h_size are the estimated blur support in the vertical and horizontal directions, respectively, and $J(m,n)$ is the autocorrelation of the image, defined by

$$J(m,n) = \frac{1}{(N-n)(M-m)} \sum_{x=n}^{N-1} \sum_{y=m}^{M-1} f(x,y) * f(x-n, y-m) \tag{4}$$

where N and M are the horizontal and vertical dimensions of the image. $f(x-n, y-m)$ is obtained by circularly shifting the image matrix n pixels in the horizontal direction and m pixels in the vertical direction.

III. Estimation of PSF Coefficients and the Restored Image

We present a joint estimation method to simultaneously solve the PSF coefficients and the restored image. This method is based on a MAP framework, and the Huber–Markov [Huber–Markov random field (HMRF)] prior model is used to regularize both the series of unknowns.

A. Construction of the Objective Function

The motivation for MAP image restoration is that it allows the posterior probability of the image and the blur to achieve the maximum, given a certain degraded image [18], [19]. That is

$$\hat{\boldsymbol{f}}, \hat{\boldsymbol{h}} = \arg\max_{\boldsymbol{f},\boldsymbol{h}} p(\boldsymbol{f}, \boldsymbol{h} | \boldsymbol{g}). \tag{5}$$

Here, the "hat" notations of $\boldsymbol{f}$ and $\boldsymbol{h}$ are used to denote the solutions of the image and the PSF in the optimization problem. Applying Bayes' formula, (5) can alternatively be expressed as

$$\hat{\boldsymbol{f}}, \hat{\boldsymbol{h}} = \arg\max_{\boldsymbol{f},\boldsymbol{h}} \frac{p(\boldsymbol{g}|\boldsymbol{f}, \boldsymbol{h}) p(\boldsymbol{f}, \boldsymbol{h})}{p(\boldsymbol{g})}. \tag{6}$$

Since the denominator on the right side has nothing to do with the solution of $\boldsymbol{f}$ and $\boldsymbol{h}$, it can be omitted. We further assume that $\boldsymbol{f}$ and $\boldsymbol{h}$ are statistically independent and impose a logarithmic function. The maximization problem is converted to minimization through the negative operation

$$\hat{\boldsymbol{f}}, \hat{\boldsymbol{h}} = \arg\min_{\boldsymbol{f},\boldsymbol{h}} \{-\log p(\boldsymbol{g}|\boldsymbol{f}, \boldsymbol{h}) - \log p(\boldsymbol{f}) - \log p(\boldsymbol{h})\}. \tag{7}$$

The most common assumption related to noise is that it can be represented by an additive independent identically distributed Gaussian model, so the conditional density $p(\boldsymbol{g}|\boldsymbol{f}, \boldsymbol{h})$ has the form

$$p(\boldsymbol{g}|\boldsymbol{f}, \boldsymbol{h}) = \frac{1}{(2\pi\sigma^2)^{MN/2}} \exp\left(\frac{-\|\boldsymbol{g} - \boldsymbol{H}\boldsymbol{f}\|_2^2}{2\sigma^2}\right) \tag{8}$$

where σ^2 is the variance of the noise and $\| \bullet \|$ denotes the $L2$-norm.

The density function $p(\boldsymbol{f})$ models the image prior. In this letter, a Huber–Markov image model [5], [20], [21] is employed. This model belongs to the Markov random field family and performs well in preserving edge and detailed information. Thus, $p(\boldsymbol{f})$ has the form of the Gibbs density function, given by

$$p(\boldsymbol{f}) = \frac{1}{Z_{\boldsymbol{f}}} \exp\left\{-\frac{1}{T_f} \sum_{c \in C} \rho_a\left(d_c^t \boldsymbol{f}\right)\right\} \tag{9}$$

where Z_f is a normalization constant, T_f is the temperature parameter, c is the clique of image pixels, C is an assembly of c, and $\rho(\bullet)$ is the Huber function, which is defined as

$$\rho_a(x) = \begin{cases} x^2, |x| \le a \\ 2a|x| - a^2, |x| > a \end{cases} \tag{10}$$

where a is the threshold that defines the separation for the quadratic and linear regions. It controls the scale and probability of the discontinuous area of the prior image. $d_c^t \boldsymbol{f}$ denotes the measures of the differences between pixels in neighborhoods of the image field. A description of their various forms can be found in [21].

In view of the belief that piecewise smoothness is not a stringent condition, we assume that the PSF also has piecewise smoothness, and we model it with the HMRF model. Thus, $p(\boldsymbol{h})$ can be given by

$$p(\boldsymbol{h}) = \frac{1}{Z_{\boldsymbol{h}}} \exp\left\{-\frac{1}{T_{\boldsymbol{h}}} \sum_{c' \in C'} \rho_{a'}\left(d_c^t \boldsymbol{h}\right)\right\} \tag{11}$$

where the parameters in (11) have the same functions as those in (9).

Substituting (8), (9), and (11) in (7) and eliminating the irrelevant constant items, the following minimization cost function is obtained:

$$\hat{\boldsymbol{f}}, \hat{\boldsymbol{h}} = \arg\min_{\boldsymbol{f},\boldsymbol{h}} \left\{ \|\boldsymbol{g} - \boldsymbol{H}\boldsymbol{f}\|_2^2 + \lambda \sum_{m=1}^{M} \sum_{n=1}^{N} \sum_{i=1}^{4} \rho_a\left(d_{m,n,i}^t \boldsymbol{f}\right) + \gamma \sum_{m=1}^{P} \sum_{n=1}^{Q} \sum_{i=1}^{4} \rho_{a'}\left(d_{m,n,i}^t \boldsymbol{h}\right) \right\} \tag{12}$$

where $\lambda = 2\sigma^2 / T_{\boldsymbol{f}}$ and $\gamma = 2\sigma^2 / T_{\boldsymbol{h}}$. The first term on the right-hand side of (12) represents the fidelity of the restored image $\boldsymbol{f}$ with respect to the observation data $\boldsymbol{g}$. Direct minimization of only this term would lead to excessive noise magnification due to the ill conditioning of the blur operator [22]. The second term narrows the solution space of $\boldsymbol{f}$ to a well-defined solution, and the λ controls the tradeoff between fidelity of the observation and smoothness of the restored image. The third term ensures that $\boldsymbol{h}$ is solved steadily.

B. Optimization Procedure

There are two sets of unknowns (image and PSF) in (12). To recover the image and identify the PSF simultaneously, an alternating minimization iterative scheme combined with a gradient descent algorithm is employed. Similar to the method described in [4], the minimum problem of (12) is decomposed into two cycling steps: estimating $\boldsymbol{f}$, assuming $\boldsymbol{h}$ is fixed, and estimating $\boldsymbol{h}$, assuming $\boldsymbol{f}$ is fixed. Before the iteration, the desired image is first initiated as $\boldsymbol{f} = \boldsymbol{g}$. Similarly, an initiated value should also be given to the PSF $\boldsymbol{h}$.

We use $L(\boldsymbol{f}, \boldsymbol{h})$ to denote the cost function of (12). For notational convenience, the subscript a of $\rho(\bullet)$ for the threshold is removed. Let $\boldsymbol{s}$ be the gradient of the cost function with respect to $\boldsymbol{f}$ and $\boldsymbol{q}$ be the corresponding conjugate vector. The detailed optimization process in relation to $\boldsymbol{f}$ with fixed $\boldsymbol{h}$ is described as follows.

1) Let $n = 0$, and initialize the conjugate vector

$$\begin{aligned}\boldsymbol{s}_0 &= \nabla_{\boldsymbol{f}} L(\boldsymbol{f}, \boldsymbol{h}) \\ &= -2\boldsymbol{H}^T(\boldsymbol{g} - \boldsymbol{H}\boldsymbol{f}) + \lambda \sum_{m=0}^{M}\sum_{n=0}^{N}\sum_{i=0}^{3} \rho_a'\left(d_{m,n,i}^t \boldsymbol{f}\right) \qquad (13)\end{aligned}$$

$$\boldsymbol{q}_0 = -\boldsymbol{s}_0. \qquad (14)$$

2) Calculate the step size for updating the image $\boldsymbol{f}$

$$\alpha_n = -\frac{\boldsymbol{q}_n^T \boldsymbol{s}_n}{\boldsymbol{q}_n^T \left(\nabla^2_{\boldsymbol{f}_n} L(\boldsymbol{f}_n, \boldsymbol{h}_n)\right) \boldsymbol{q}_n}. \qquad (15)$$

3) Update $\boldsymbol{f}$

$$\boldsymbol{f}_{n+1} = \boldsymbol{f}_n + \alpha_n \boldsymbol{q}_n. \qquad (16)$$

4) Update the gradient of the cost function with respect to $\boldsymbol{f}$

$$\boldsymbol{s}_{n+1} = \nabla_{\boldsymbol{f}} L(\boldsymbol{f}_{n+1}, \boldsymbol{h}_n). \qquad (17)$$

5) Calculate the step size for updating the conjugate vector

$$\tau_n = \frac{\boldsymbol{q}_n^T \left(\nabla^2_{\boldsymbol{f}_{n+1}} L(\boldsymbol{f}_{n+1}, \boldsymbol{h}_n)\right) \boldsymbol{s}_{n+1}}{\boldsymbol{q}_n^T \left(\nabla^2_{\boldsymbol{f}_{n+1}} L(\boldsymbol{f}_{n+1}, \boldsymbol{h}_n)\right) \boldsymbol{q}_n}. \qquad (18)$$

6) Update the conjugate vector

$$\boldsymbol{q}_{n+1} = -\boldsymbol{s}_{n+1} + \tau_n \boldsymbol{q}_n. \qquad (19)$$

7) $n = n + 1$. The iteration is terminated when

$$\frac{\|\boldsymbol{f}_{n+1} - \boldsymbol{f}_n\|_2^2}{\|\boldsymbol{f}_n\|_2^2} < \varepsilon \qquad (20)$$

where ε is a predetermined value. Otherwise, go to step 2).

The conjugate-gradient optimization method is also employed to solve the PSF $\boldsymbol{h}$. The solution steps are similar to that of (13)–(20), replacing $\boldsymbol{H}$ and $\boldsymbol{f}$ with $\boldsymbol{F}$ and $\boldsymbol{h}$. Here, $\boldsymbol{F}$ is a sparse matrix which satisfies $\boldsymbol{F}\boldsymbol{h} = \boldsymbol{H}\boldsymbol{f}$. In order to relieve the effects derived by the ill-posed problem, the following constraints on $\boldsymbol{f}$ and $\boldsymbol{h}$ are respectively imposed in each iteration:

$$\min \le f(m,n) \le \max \qquad (21)$$

$$\sum h(i,j) = 1, h(i,j) \ge 0, \qquad h(i,j) = h(-i,-j). \qquad (22)$$

IV. Experimental Results

In this section, the proposed support estimation method and restoration method are tested using both simulated and real images. To quantitatively evaluate the restored images, the three metrics of the peak signal-to-noise ratio (PSNR), the universal image quality index (UIQI) [23], and the metric Q [24] are employed. Among these three metrics, the PSNR and UIQI, whose ideal values are $+\infty$ and 1, respectively, require the existence of a reference image. Therefore, they can only be used in simulated experiments. The metric Q, which is a no-reference measure of image content, can also be used in the experiments performed on real images. It has been verified that metric Q can reflect the amount of both blur and noise, without any prior knowledge [24]. The larger the value of Q, the higher the image quality.

TABLE I
Results of Different Methods With Actual Support 5 × 5

Image \ σ		1.6	1.8	2.0	2.5	3.0	5.0
cameraman	MCSC	4×5	4×5	5×5	5×5	5×5	5×5
	Proposed	5×3	5×5	5×5	5×5	5×5	5×5
peppers	MCSC	4×5	5×4	5×5	5×5	5×5	5×5
	Proposed	4×4	5×4	5×5	5×5	5×5	5×5
Lena	MCSC	4×5	4×5	5×5	5×6	5×6	5×6
	Proposed	5×4	5×4	5×5	5×5	5×5	5×5

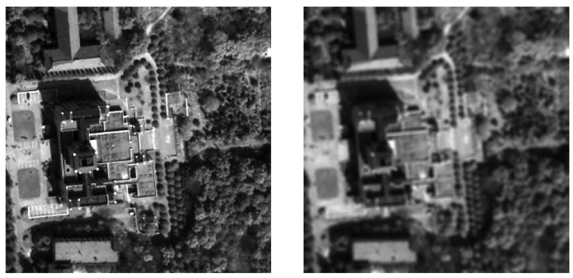

(a) (b)

Fig. 2. QuickBird test image. (a) Original image and (b) blurred image.

A. Performance Validation of Support Estimation

The simulations on the standard test images of "cameraman," "peppers," and "Lena" are first presented to demonstrate the effectiveness of the PSF support estimation method. A series of experiments with different standard deviations σ and support 5×5 was performed. The proposed method is compared to the MCSC method in [17]. The estimation results are shown in Table I. It is seen that the proposed method has a similar performance to minimum cyclic-shift correlation (MCSC). In some cases, it provides better results with lower computational complexity. For a 256×256 image, the computational times of the proposed method and MCSC are 0.12 and 0.17 s, respectively, on a common portable computer. For both methods, the time spent is proportional to image size.

The performance of the PSF support estimation method was also tested using a preprocessed high-quality QuickBird remote sensing image, as shown in Fig. 2(a). The images used in the restoration process are cropped subimages of 300×300 pixels. Fig. 2(b) is a low-pass-filtered (5×5 Gaussian blur, standard deviation of $\sigma = 2.1$) image. The correlation curves of $J(m, 0)$ and $J(0, n)$ are shown in Fig. 3. It is clearly observed that the curves attain their minimum at shift distance 5 in both directions.

B. Performance Validation of the Restoration Method

The proposed iterative restoration method was tested on both noise-free images and noisy images. In the noise-free case, the

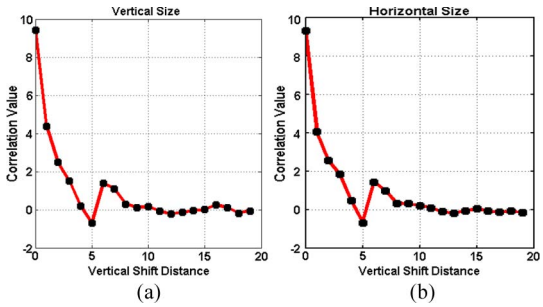

Fig. 3. Correlation curves. (a) Result of Fig. 2(b) in the vertical direction and (b) result of Fig. 2(b) in the horizontal direction.

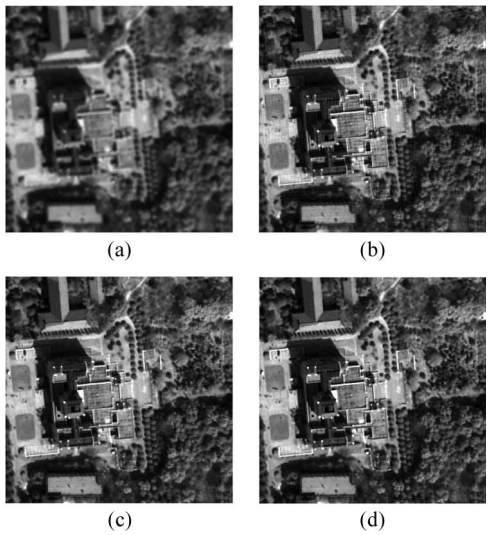

Fig. 4. Restored results in the noise-free case. (a) Degraded image by 5×5 Gaussian blur, (b) restored image of the IBD method, (c) restored image of the MLO method, and (d) restored image of the proposed method.

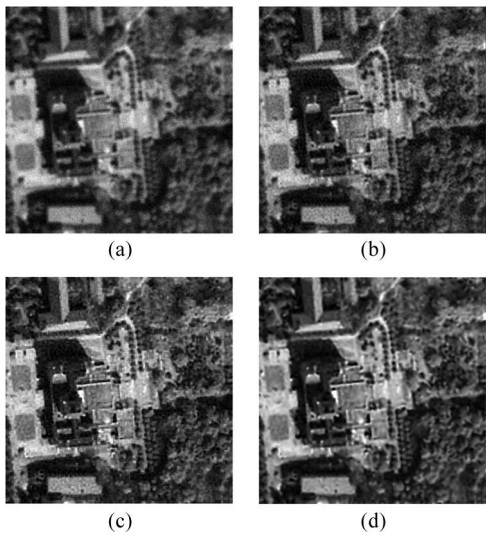

Fig. 5. Restored results in the noisy case. (a) Degraded image by 5×5 Gaussian blur and Gaussian noise, with SNR being 20 dB, (b) restored image of the IBD method, (c) restored image of the MLO method, and (d) restored image of the proposed method.

input image [Fig. 4(a)] was obtained by degrading the original image by a 5×5 Gaussian blur, with the standard deviation σ being 2.1. In the noisy case, the input image [Fig. 5(a)] was obtained by adding Gaussian noise $(SNR = 20$ dB$)$ to the blurred image. In order to demonstrate the performance of the proposed restoration method, it was compared to the IBD method [13], the MLD method [15], and the MLO method [12]. All the four restoration methods are given the same initial PSF coefficients, which correspond to a Gaussian blur with $\sigma = 1.6$.

TABLE II
EVALUATION RESULTS OF DIFFERENT ALGORITHMS

Image	Noise-free case			Noisy case		
	PSNR	UIQI	Q	PSNR	UIQI	Q
Degraded	22.719	0.943	41.76	21.465	0.926	18.81
IBD	27.712	0.984	45.90	22.559	0.944	30.86
MLD	26.742	0.980	45.33	22.194	0.940	27.47
MLO	31.147	0.993	46.81	23.342	0.955	39.32
Proposed	32.544	0.995	48.07	23.782	0.959	46.14

TABLE III
ACTUAL PSF COEFFICIENTS

0.0245	0.0345	0.0386	0.0345	0.0245
0.0345	0.0484	0.0543	0.0484	0.0345
0.0386	0.0543	0.0608	0.0543	0.0386
0.0345	0.0484	0.0543	0.0484	0.0345
0.0245	0.0345	0.0386	0.0345	0.0245

TABLE IV
ESTIMATED PSF COEFFICIENTS OF FIG.4(a)

0.0276	0.0335	0.0393	0.0336	0.0278
0.0347	0.0446	0.0537	0.0446	0.0348
0.0412	0.0537	0.0618	0.0537	0.0412
0.0348	0.0446	0.0537	0.0446	0.0347
0.0278	0.0336	0.0393	0.0335	0.0276

TABLE V
ESTIMATED PSF COEFFICIENTS OF FIG.5(a)

0.0259	0.0287	0.0321	0.0297	0.0272
0.0399	0.0470	0.0506	0.0475	0.0406
0.0467	0.0549	0.0586	0.0549	0.0467
0.0406	0.0475	0.0506	0.0470	0.0399
0.0272	0.0297	0.0321	0.0287	0.0259

The restored results are shown in Figs. 4 and 5, respectively. Since the results of the MLD and IBD methods are visually similar, we only display the IBD images and do not display the MLD images. From Fig. 4, we can see that the proposed method produces much sharper images than the other methods. Fig. 5 shows that the proposed method is less sensitive to noise. The evaluation results are shown in Table II. It is seen that, regardless of the presence or absence of noise, the values of the PSNR and UIQI indices of the proposed method are higher than those of the other methods. It can also be seen that the Q index has a similar trend to the PSNR and UIQI indices, which validates the good performance of this no-reference metric. Therefore, it is used to evaluate the restored results of the real images in the next section. The actual PSF coefficients are shown in Table III.

Tables IV and V are the estimated PSF coefficients of the proposed method. It is shown that the estimated coefficients have very small errors.

C. Application to CBERS-02B Panchromatic Images

Finally, the proposed algorithm was applied to real remote sensing images. Ten subimages were cropped from three original panchromatic images of the The 2B satellite of the China–Brazil Earth Resources Satellite Program (CBERS-2B) high-resolution camera. In order to save space, only two of them are illustrated. Fig. 6 shows the estimated PSFs, and the original

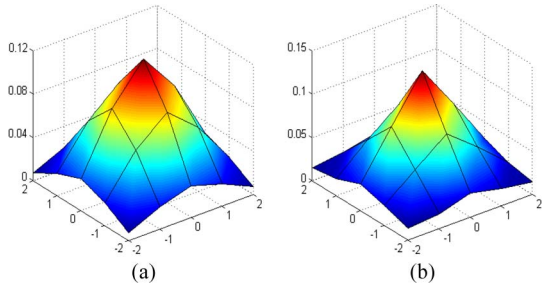

Fig. 6. Estimated PSF functions of the CBERS-2B images. (a) PSF of Fig. 7(a) and (b) PSF of Fig. 7(c).

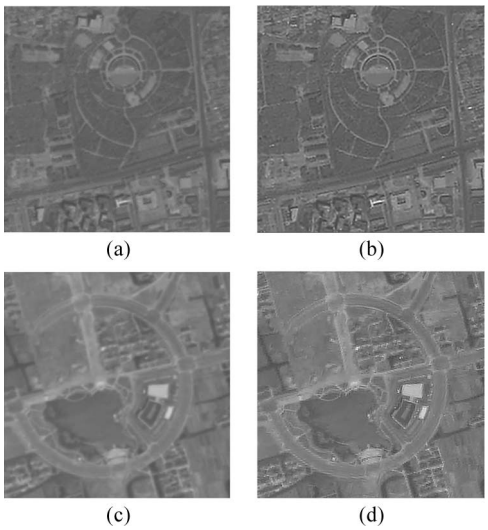

Fig. 7. Restored results of the CBERS-2B panchromatic images. (a) and (c) Original images. (b) and (d) Restored images of the proposed method.

TABLE VI
QUANTITATIVE COMPARISON OF THE ORIGINAL AND RESTORED CBERS-2B IMAGES, USING THE Q METRIC

	Original	IBD	MLD	MLO	Proposed
Image 1	12.42	20.71	21.48	22.63	**24.15**
Image 2	13.61	14.62	14.67	**18.26**	18.22
Image 3	21.48	35.81	41.51	43.56	**46.56**
Image 4	15.16	22.32	27.64	28.97	**30.61**
Image 5	17.30	24.62	36.07	36.70	**42.22**
Image 6	14.11	18.31	27.77	29.71	**30.67**
Image 7	10.28	15.24	22.90	24.33	**25.83**
Image 8	6.950	10.40	15.09	16.21	**16.72**
Image 9	26.59	36.94	52.53	56.31	**59.30**
mage 10	12.91	20.73	27.53	29.75	**31.26**

images and restored results are shown in Fig. 7. It is obvious, by visual inspection, that the original CBERS-2B panchromatic images are blurred to a considerable extent, and the proposed method produces much clearer images. Table VI shows the Q values of all the ten subimages. It is seen that all the blind restoration methods raise the Q index, but the proposed method obtains the highest values for nine of the ten images.

V. CONCLUSION

This letter has presented a new restoration method for the deblurring of remote sensing images. We have proposed a PSF support estimation method and a blind restoration method. Experimental results showed that these methods perform quite well in terms of both visual inspection and quantitative evaluation. Because of the employment of a complicated prior model, however, the proposed iterative restoration method has considerable computational complexity. For example, the proposed method is up to ten times slower than the IBD and MLD methods. Therefore, further work could potentially improve the processing efficiency of the proposed method.

REFERENCES

[1] W. H. Richardson, "Bayesian-based iterative method of image restoration," *J. Opt. Soc. Amer.*, vol. 62, no. 1, pp. 55–59, 1972.

[2] L. Lucy, "An iterative technique for the rectification of observed distributions," *Astron. J.*, vol. 79, no. 6, pp. 745–765, Jun. 1974.

[3] Z. Liu, C. Wang, and C. Luo, "CBERS-1 PSF estimation and image restoration," *J. Remote Sens.*, vol. 8, no. 3, pp. 234–238, 2004.

[4] Y. You and M. Kaveh, "A regularization approach to joint blur identification and image restoration," *IEEE Trans. Image Process.*, vol. 5, no. 3, pp. 416–428, Mar. 1996.

[5] R. Pan and S. Reeves, "Efficient Huber–Markov edge-preserving image restoration," *IEEE Trans. Image Process.*, vol. 15, no. 12, pp. 3728–3735, Dec. 2006.

[6] J. Papa, N. Mascarenhas, L. Fonseca, and K. Bensebaa, "Convex restriction sets for CBERS-2 satellite image restoration," *Int. J. Remote Sens.*, vol. 29, no. 2, pp. 443–458, Jan. 2008.

[7] Y. Lou, A. L. Bertozzi, and S. Soatto, "Direct sparse deblurring," *J. Math. Imag. Vis.*, vol. 39, no. 1, pp. 1–12, Jan. 2011.

[8] M. Zhao, W. Zhang, Z. Wang, and Q. Hou, "Satellite image deconvolution based on nonlocal means," *Appl. Opt.*, vol. 49, no. 32, pp. 6286–6294, Nov. 2010.

[9] M. Cannon, "Blind deconvolution of spatially invariant image blurs with phase," *IEEE Trans. Acoust., Speech, Signal Process.*, vol. ASSP-24, no. 1, pp. 58–63, Feb. 1976.

[10] R. Ryan, B. Baldridge, R. Schowengerdt, T. Choi, D. Helder, and S. Blonski, "IKONOS spatial resolution and image interpretability characterization," *Remote Sens. Environ.*, vol. 88, no. 1/2, pp. 37–52, Nov. 2003.

[11] T. Choi, "IKONOS satellite on orbit Modulation Transfer Function (MTF) measurement using edge and pulse method," M.S. thesis, Elect. Eng. Dept., South Dakota State Univ., Brookings, SD, 2002.

[12] A. Levin, Y. Weiss, F. Durand, and W. T. Freeman, "Efficient marginal likelihood optimization in blind deconvolution," in *Proc. IEEE CVPR*, 2011, pp. 2657–2664.

[13] G. Ayers and J. Dainty, "Iterative blind deconvolution method and its applications," *Opt. Lett.*, vol. 13, no. 7, pp. 547–549, Jul. 1988.

[14] D. Fish, A. Brinicombe, E. Pike, and J. Walker, "Blind deconvolution by means of the Richardson–Lucy algorithm," *J. Opt. Soc. Amer. A, Opt. Image Sci.*, vol. 12, no. 1, pp. 58–65, Jan. 1995.

[15] T. J. Holmes, S. Bhattacharyya, J. A. Cooper, D. Hanzel, V. Krishnamurthi, W. Lin, B. Roysam, D. H. Szarowski, and J. N. Turner, "Light microscopic images reconstructed by maximum likelihood deconvolution," in *Handbook of Biological Confocal Microscopy*. Berlin, Germany: Springer-Verlag, 1995, pp. 389–402.

[16] X. Chen, S. Yang, X. Wang, and Y. Qiao, "Satellite image blind restoration based on surface fitting and iterative multishrinkage method in redundant wavelet domain," *Optik, Int. J. Light Electron Opt.*, vol. 121, no. 21, pp. 1909–1911, Nov. 2010.

[17] L. Chen and K. Yap, "Efficient discrete spatial techniques for blur support identification in blind image deconvolution," *IEEE Trans. Signal Process.*, vol. 54, no. 4, pp. 1557–1562, Apr. 2006.

[18] Q. Yuan, L. Zhang, H. Shen, and P. Li, "Adaptive multiple-frame image super-resolution based on U-curve," *IEEE Trans. Image Process.*, vol. 19, no. 12, pp. 3157–3170, Dec. 2010.

[19] H. Shen, L. Zhang, B. Huang, and P. Li, "A MAP approach for joint motion estimation, segmentation, and super resolution," *IEEE Trans. Image Process.*, vol. 16, no. 2, pp. 479–490, Feb. 2007.

[20] L. Zhang, Q. Yuan, H. Shen, and P. Li, "Multiframe image super-resolution adapted with local spatial information," *J. Opt. Soc. Amer. A, Opt. Image Sci.*, vol. 28, no. 3, pp. 381–390, Mar. 2011.

[21] H. Shen, M. K. Ng, P. Li, and L. Zhang, "Super resolution reconstruction algorithm to MODIS remote sensing images," *Comput. J.*, vol. 52, no. 1, pp. 90–100, Jan. 2009.

[22] L. Chen and K. Yap, "A soft double regularization approach to parametric blind image deconvolution," *IEEE Trans. Image Process.*, vol. 14, no. 5, pp. 624–633, May 2005.

[23] Z. Wang and A. Bovik, "A universal image quality index," *IEEE Signal Process. Lett.*, vol. 9, no. 3, pp. 81–84, Mar. 2002.

[24] X. Zhu and P. Milanfar, "Automatic parameter selection for denoising algorithms using a no-reference measure of image content," *IEEE Trans. Image Process.*, vol. 19, no. 12, pp. 3116–3132, Dec. 2010.